Optica Applicata, Vol. XI, No. 3, 1981

A numerical illustration of the shape influence of both the shape and boundary distribution in reconstructed image region on the direct recovery error*

RENATA NOWAK, IRENEUSZ WILK

Institute of Physics, Technical University of Wrocław, Wybrzeże Wyspiańskiego 27, 50-370 Wrocław, Poland.

The direct recovery method of incoherent image reconstruction from sampling data was proposed in papers [1–5]**. One of the problems so far unsolved is the influence of both the shape and boundary points distribution in the sampled image region on the direct reconstruction error. Although it is quite clear that for large-area regions of regular shape this influence may be negligible outside some (small) boundary regions, the problem may become serious for very small areas containing small number of sampling points.

Instead of developing a general theory to clarify this situation we prefer to illustrate it with some numerical examples allowing to gain some intuition in this direction.

The numerical calculations were performed for three types of recovered image regions. All the regions a square, a rectangular and a trapezium-on-rectangle combination were of almost the same area (the differences being less than 6.5%) and had almost the same number of sampling points (table 1). The positions of both the sampling points and the image points are illustrated in fig. 1.

Table 1. Parameters of the compared image fragments

Investigated region	Surface [mm^2]	Number of sampling points	Number of boundary points
Square (I)	$0.655 \cdot 10^{-3}$	25	9
Rectangle (II)	$0.614 \cdot 10^{-3}$	24	9
Trapezium-on-rectangle (III)	$0.655 \cdot 10^{-3}$	24	10

For all the three cases the same sampling step ($d = 0.0032$ mm) and the same light wavelength ($\lambda = 0.00058$ nm) were assumed.

All the calculations contained in this work have been done under assumption that the imaging system of 4.5 f-number is diffraction-limited [4], while the object is positioned at infinity. Also it has been assumed that the measurement results at the sampling points inside the recovered region are normed to the value $1 \cdot 10^{-6}$, while those at the boundary, are equal to half of this value, as illustrated in fig. 1.

The optical sampling system is reduced to the integrating element itself [2, 4] being a circle of radius $R_E = 0.0032$ mm.

As indicated earlier [4] such reduction of the sampling system for the case of aberration-less imaging system results only in slight quantitative changes in the sets of reconstructed intensity values.

* This work was carried on under the Research Project M.R. I.5.

** This letter is a supplement of the paper [4], and should be read jointly with the latter.

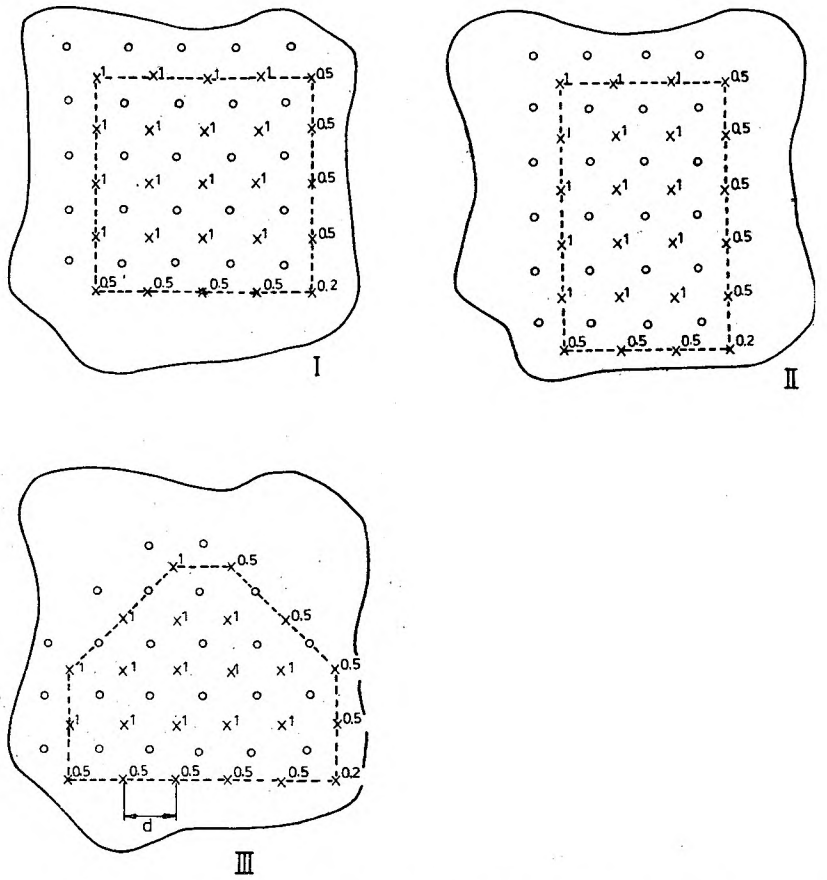

Fig. 1. Set of measurement (×) and imaged (○) points in the case of lower-bounded reconstruction the imaged points lying between the measurement points. The shape of the region to be recovered is marked with a solid line. d – sampling step. The numbers denote the postulated measurement results at the sampling points magnified 10^6 times

The reconstructed distributions of intensity at the sampling points as well as the reconstruction errors for the said three shapes of recovered image regions are shown in tables 2–4.

As may be seen the direct recovery method is almost insensitive to the shape changes in the reconstructed image region for the cases considered. The reconstruction errors, at the points lying within the region, especially in its central part, are approximately the same for the square, the rectangle, and the trapezium-on-rectangle combination if the sampling and lower-bound reconstruction imaging points are positioned as shown in fig. 1.

The other problem in the recovery procedure is the proper choise of the boundary points in the lower-bound reconstruction. The configuration of these points may be different as illustrated in fig. 2, for a rectangular image recovered.

The performed calculations have shown that the change in configuration of boundary points has no essential influence on the direct reconstruction error values in the central part of the recovered image region. However, the reconstruction errors in the boundary zone may be considerably influenced, which is illustrated in table 5.

Table 2. The upper-bound (I_{max}) and lower-bound (I_{min}) intensity distribution and the reconstruction errors ΔI for the region I

Region I (square)														
$I^{max}[\times 10^{-2}]$						$I^{min}[\times 10^{-2}]$				$\Delta I = 0.5\|(I^{max} - I^{min})\|[\times 10^{-2}]$				
9.945	3.803	5.972	8.192	1.718	1.811	1.841	1.841	1.811	0.923	4.067	0.981	2.065	3.190	0.397
3.803	5.093	3.971	3.775	2.682	1.841	1.816	1.886	1.841	0.946	0.981	1.638	1.042	0.967	0.867
5.972	3.971	3.958	5.651	1.746	1.841	1.886	1.886	1.841	0.946	2.065	1.042	1.036	1.905	0.400
8.192	3.775	5.651	6.757	1.588	1.811	1.841	1.841	1.811	0.931	3.190	0.966	1.905	2.473	0.328
1.719	2.681	1.746	1.589	2.231	0.923	0.946	0.946	0.923	0.564	0.397	0.867	0.400	0.333	0.833

Table 3. The upper-bound (I^{max}) and lower-bound (I^{min}) intensity distribution and reconstruction errors ΔI for the region II

Region II (rectangle)												
$I^{max}[\times 10^{-2}]$				$I^{min}[\times 10^{-2}]$				$\Delta I = 0.5\|(I^{max} - I^{min})\|[\times 10^{-2}]$			
9.651	3.623	7.797	1.761	1.795	1.795	1.795	1.011	3.928	0.914	3.001	0.375
3.623	5.016	3.641	2.628	1.795	1.812	1.795	1.03(	0.914	1.602	0.923	0.799
5.895	3.928	3.875	2.186	1.795	1.812	1.795	1.02(	2.050	1.058	1.040	0.579
7.737	3.888	3.919	1.878	1.795	1.812	1.795	1.02(	3.001	1.038	1.062	0.428
7.993	3.629	4.195	1.762	1.795	1.801	1.811	1.030	3.099	0.914	1.192	0.366
1.761	2.570	1.660	3.265	1.011	1.032	1.030	1.663	0.375	0.767	0.315	0.801

Table 4. The upper-bound (I^{max}) and lower-bound (I^{min}) intensity distribution and the reconstruction errors ΔI for the region III

Region III (trapezium-on-rectangle combination)																	
I^{max} [$\times 10^{-2}$]							I^{min} [$\times 10^{-2}$]					$\Delta I = 0.5\|(I^{max} - I^{min})\|$ [$\times 10^{-2}$]					
		2.569	1.556					1.439	0.412					0.565	0.572		
	4.546	5.315	5.447	1.625			1.460	1.475	1.460	0.741			1.543	1.920	1.993	0.442	
6.568	3.821	3.801	3.795	3.846	1.628	1.748	1.791	1.781	1.791	1.750	0.846	2.410	1.015	1.010	1.002	1.048	0.388
7.537	3.918	5.440	5.556	4.017	1.486	1.795	1.756	1.756	1.756	1.795	0.840	2.871	1.081	1.842	1.900	1.111	0.323
1.540	2.366	1.643	1.601	1.433	1.468	0.832	0.844	0.841	0.839	0.831	0.420	0.354	0.761	0.401	0.381	0.301	0.524

Table 5. Comparison of the reconstruction errors for three different configurations of the boundary points (see also fig. 2)

Configuration A					Configuration B					Configuration C				
$\Delta I = 0.5\|(I^{max} - I^{min})\|$ [$\times 10^{-2}$]					$\Delta I = 0.5\|(I^{max} - I^{min})\|$ [$\times 10^{-2}$]					$\Delta I = 0.5\|(I^{max} - I^{min})\|$ [$\times 10^{-2}$]				
0.522	0.884	0.842	0.311	0.522	0.681	0.903	1.963	2.914	0.558	4.967	0.981	2.065	3.190	0.397
0.813	1.580	1.021	1.039	0.843	0.856	1.572	1.018	0.994	0.810	0.981	1.603	1.042	0.967	0.867
0.971	1.023	1.012	1.811	0.891	0.995	1.018	1.028	1.894	0.951	2.065	1.042	1.036	1.905	0.400
2.910	1.040	1.810	1.976	0.981	0.648	0.994	1.894	2.079	0.653	3.190	0.966	1.905	2.473	0.333
0.357	0.722	1.093	1.002	0.824	0.579	0.803	1.477	0.978	0.532	0.397	0.867	0.400	0.333	0.835

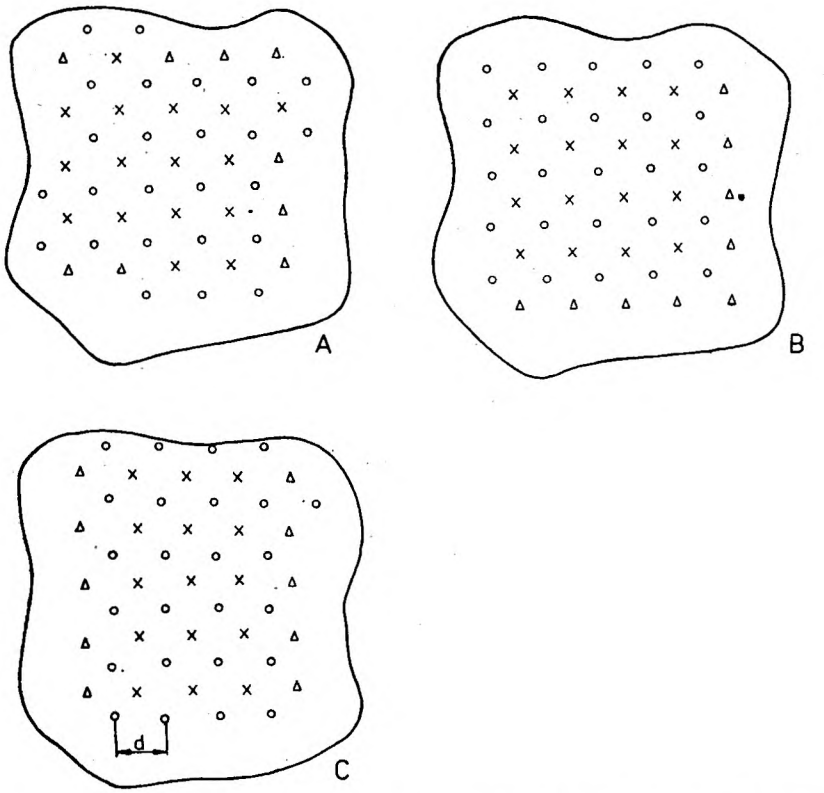

Fig. 2. Sets of measurement (×) and imaged (○) points in the case of the lower-bound reconstruction. The triangles denote the boundary points of the region. Letters A, B, C denote different types of boundary-points configurations

References

[1] Wilk I., Pr. nauk. Inst. Fizyki PWr., No. 4, Studia i Materiały No. 4, Wrocław 1970.
[2] Wilk I., Pr. nauk. Inst. Fizyki PWr., No. 2, Studia i Materiały No. 2, Wrocław 1969. p. 9.
[3] Wilk I., Zeszyty Naukowe PWr., Fizyka **XV**, Wrocław 1969, p. 11.
[4] Nowak R., Wilk I., Optica Applicata **X** (1980).
[5] Wilk I., Nowak R., Optica Applicata **XI** (1981) in press.

Received September 3, 1980